HHS Public Access

Author manuscript

Immunity. Author manuscript; available in PMC 2020 January 15.

Published in final edited form as:

Immunity. 2019 January 15; 50(1): 51–63.e5. doi:10.1016/j.immuni.2018.12.013.

Oligoadenylate synthetases family protein OASL inhibits DNA sensor cGAS activity during DNA virus infection to limit interferon production.

Arundhati Ghosh[1,2], **Lulu Shao**[1,2], **Padmavathi Sampath**[1,3], **Baoyu Zhao**[4], **Nidhi V. Patel**[1], **Jianzhong Zhu**[†,1,2], **Bharat Behl**[5], **Robert A. Parise**[6], **Jan H. Beumer**[6], **Roderick J. O'Sullivan**[7], **Neal A. DeLuca**[1,2], **Stephen H. Thorne**[1,3], **Vijay A.K. Rathinam**[5], **Pingwei Li**[4], and **Saumendra N. Sarkar**[*,1,2]

[1]Cancer Virology Program, University of Pittsburgh Cancer Institute, University of Pittsburgh School of Pharmacy, Pittsburgh, PA.

[2]Department of Microbiology and Molecular Genetics, University of Pittsburgh School of Pharmacy, Pittsburgh, PA.

[3]Department of Cell Biology, University of Pittsburgh School of Pharmacy, Pittsburgh, PA.

[7]Department of Pharmacology and Chemical Biology, University of Pittsburgh School of Medicine, University of Pittsburgh School of Pharmacy, Pittsburgh, PA.

[6]Department of Pharmaceutical Sciences, University of Pittsburgh School of Pharmacy, Pittsburgh, PA.

[4]Department of Biochemistry and Biophysics, Texas A&M University, College Station, TX

[5]Department of Immunology, UConn Health School of Medicine, Farmington, CT

SUMMARY

Interferon-inducible human oligoadenylate synthetases-like (*OASL*) and its mouse orthologue *Oasl2* enhance RNA-sensor RIG-I-mediated type I interferon (IFN) induction and inhibit RNA virus replication. Here we show that *OASL* and *Oasl2* have the opposite effect in the context of DNA virus infection. In *Oasl2*$^{-/-}$ mice and *OASL*-deficient human cells, DNA viruses, such as Vaccinia, Herpes simplex and Adenovirus induced increased IFN production, which resulted in

[*]Lead Contact: Saumendra N. Sarkar, Ph.D., University of Pittsburgh Cancer Institute, Hillman Cancer Research Pavilion, Suite 1.8, 5117 Centre Avenue, Pittsburgh, PA 15213, Phone: (412) 623-7720, Fax: (412) 623-7715, saumen@pitt.edu.

AUTHOR CONTRIBUTIONS

AG and SNS conceived and oversaw the whole study. AG along with LS and JZ carried out most experiments. AG, PS and SHT were involved in the VV experiments. NVP, BZ and PL helped with purified proteins and cGAS assays with additional help from RAP and JHB. NAD helped with HSV-d109 and RNAseq experiments. VR and BB helped to carry out cGAS immunofluorescence. SNS with help from AG and other authors wrote the manuscript.

† Current Address: College of Veterinary Medicine, Yangzhou University, Yangzhou, China

DECLARATION OF INTEREST

PS and SHT are full time employees and may have ownership interests at Western Oncolytics at present. However, the work presented here were carried out while they were at the University of Pittsburgh and no part of this work was carried out at the company.

reduced virus replication and pathology. Correspondingly, ectopic expression of *OASL* in human cells inhibited IFN induction through the cGAS-STING DNA-sensing pathway. cGAS was necessary for the reduced DNA virus replication observed in *OASL*-deficient cells. OASL directly and specifically bound to cGAS independent of double-stranded DNA, resulting in a non-competitive inhibition of the second messenger cyclic GMP-AMP production. Our findings define distinct mechanisms by which OASL differentially regulates host IFN responses during RNA and DNA virus infection and identify OASL as a negative-feedback regulator of cGAS.

Graphical Abstract

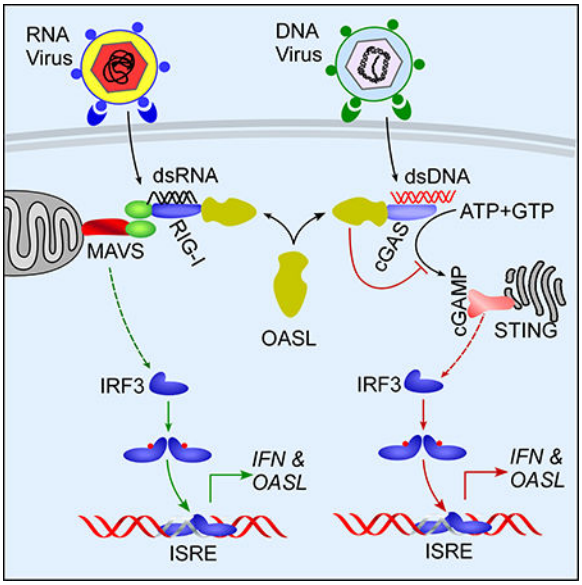

INTRODUCTION

Nucleic acid sensors of the innate immune system initiate cellular innate immune response upon sensing viral nucleic acids. While the RNA viruses primarily are sensed through the RIG-I-like receptors (RLR) and Toll-like receptors (TLR), a growing body of evidence has now shown the critical importance of the cyclic GMP-AMP synthase (cGAS) – stimulator of Interferon gene (STING) sensing pathway in sensing the majority of DNA viruses (Hartmann, 2017). In both RLR and cGAS-STING pathway, the respective adaptors MAVS and STING promote interferon regulatory factor 3 (IRF3) activation and type I Interferon (IFN) production. cGAS is an enzyme belonging to the ancient Oligoadenylate Synthase (OAS) family proteins (Sun et al., 2012; Kranzusch et al., 2015). cGAS is activated upon binding DNA and synthesizes unique second messenger molecule 2’−5’ cyclic GMP-AMP (cGAMP). cGAMP binds to the adaptor protein STING resulting its activation and downstream IFN induction (Chen et al., 2016). IFN in an autocrine and paracrine manner induces a large number of genes, IFN-stimulated genes (ISGs) providing the cellular antiviral immunity to the surrounding cells and further shaping the adaptive immunity. Although multiple mechanisms for modulation of the RNA-sensing pathway by various ISGs has been documented, specific modulation of the DNA-sensing pathway by ISG is not well understood.

Recent structural studies have shown that upon binding to DNA through its N-terminal domain cGAS oligomerizes, which leads to conformational change and activation of its enzyme activity (Li et al., 2013; Civril et al., 2013; Diner et al., 2013; Gao et al., 2013; Hornung et al., 2014; Andreeva et al., 2017). The active enzyme synthesizes cGAMP in two-steps by a non-processive mechanism (Hornung et al., 2014). Besides causing STING activation in the same cell, cGAMP can also spread to neighboring cells and activate STING (Ablasser et al., 2013). Furthermore, given the role of cGAS in regulating cellular senescence (Dou et al., 2017; Glück et al., 2017; Mackenzie et al., 2017), regulation of the cGAS activity is crucial for the cellular homeostasis. However, besides regulation of cGAS transcription by IFN, few mechanisms are known for the regulation of cGAS activity. Beyond generalized regulation of cGAS protein through ubiquitination (Hu et al., 2016), polyglutamylation of cGAS was shown to affect its DNA binding activity, thereby inhibiting cGAMP synthesis (Xia et al., 2016). However, the biological context of some of these regulations has remained unclear.

The primary mechanism of antiviral activity of IFN-inducible OAS family proteins has been ascribed to the ability to synthesize 2'−5' oligoadenylates, and activate the latent RNase L leading to the inhibition of protein synthesis (Kristiansen et al., 2011). However, the antiviral activity of multiple enzymatically inactive members of this family cannot be explained by this simple model. Additionally, the finding that only one human OAS isozyme OAS3 is important for RNase L activation raised further questions about the mechanism of action of these proteins (Li et al., 2016). Human Oligoadenylate synthase-like (OASL) is a member of OAS family proteins without OAS enzyme activity. We have shown that the antiviral activity of OASL against a number of RNA viruses is mediated through its unique ability to interact and enhance RIG-I activation by viral RNA (Zhu et al., 2014). We also demonstrated that among the two mouse *Oasl* genes – *Oasl1* and *Oasl2*, *Oasl2* is the functional equivalent of human *OASL* and exerts antiviral activity against RNA viruses through the same mechanism (Dhar et al., 2015; Zhu et al., 2014). A number of OASL orthologs from different mammalian and bird species also exhibit antiviral activity (Chen et al., 2017a; Oh et al., 2016; Zheng et al., 2016). However, the effect of the OASL in the context of DNA virus infection specifically on the DNA-sensing pathway remained unexplored.

Here we describe an additional regulatory function of the OASL system where it works differently in the context of DNA virus infection. OASL inhibits IFN induction *in vivo* and *in vitro* during DNA virus infections, which is opposite to its IFN-promoting antiviral activity against RNA virus infection. Consequently, in the absence of OASL IFN induction is enhanced and acute virus replication is reduced for a number of DNA viruses. We found that OASL binds to cGAS and inhibits cGAMP synthesis. In summary, during DNA virus infection OASL works as a negative regulator of the cGAS-STING signaling to limit type I IFN response.

RESULTS

Mouse *Oasl2* differentially regulates RNA and DNA virus replication.

Human *OASL* was shown to have antiviral activity against several RNA viruses. However, its antiviral activity was not apparent against DNA viruses (Schoggins et al., 2011, 2014).

We established the functional equivalency of human *OASL* and mouse *Oasl2*$^{-/-}$, and showed that *in vitro* replication of vesicular stomatitis virus (VSV), a negative-strand RNA virus, was enhanced in bone marrow-derived macrophages (BMDMs) derived from *Oasl2*$^{-/-}$ mice (Dhar et al., 2015; Zhu et al., 2014). To establish the antiviral activity of *OASL in vivo* we used the *Oasl2*$^{-/-}$ mice and an intranasal VSV challenge model (Nair et al., 2014). As expected, *Oasl2*$^{-/-}$ mice exhibited increased VSV replication in the brain, indicated by enhanced green fluorescent protein (GFP) expression (Fig. 1A) and increased levels of VSV transcript (Fig. 1B) on the post-infection day 4. These results provide *in vivo* validation of our observation that *Oasl2* imparts antiviral activity against RNA viruses.

To understand the role of *Oasl2* during DNA virus infection we used Vaccinia virus (VV) model (Ablasser et al., 2013; Li et al., 2013a). Two groups of age-matched mice (N=8) were intranasally infected with VV carrying a luciferase reporter (VV-Luc) (Kirn et al., 2007). *In vivo* viral gene expression was monitored by bioluminescence. Unlike VSV, *Oasl2*$^{-/-}$ mice showed a substantially reduced viral replication compared to the WT mice (Fig. 1C), indicating that *Oasl2* did not provide protection against VV infection, rather enhanced susceptibility. Virus replication was reduced at the site of inoculation (Fig 1D), and virus spread in the lung was also reduced (Fig. 1E). The *Oasl2*$^{-/-}$ mice showed reduced pathogenesis as measured by the loss of body weight compared to the WT mice (Fig. 1F). These results indicate that *Oasl2* plays opposite roles *in vivo* during RNA vs DNA virus infection: while *Oasl2* protects against RNA virus infection in the context of DNA virus infection, the absence of *Oasl2* leads to reduced virus replication.

Human *OASL* and mouse *Oasl2* promote DNA virus replication

Next, we investigated the differential impact of *Oasl2* and human *OASL* in other DNA virus infections using *in vitro* models. Corroborating our *in vivo* observation, VV-Luc replication was significantly reduced in primary fibroblasts from the *Oasl2*$^{-/-}$ mice, compared to the WT controls (Fig. 2A, Fig. S1A). Furthermore, we infected genome edited human BJ-Tert cells (Fig. S1B, unless mentioned otherwise, BJ-tert OASL-KO clone #3 was used for all the experiments), which are immortalized human fibroblasts, with VV-Luc. Here again, *OASL*-deficient cells (OASL-KO) showed a significant decrease in VV-Luc replication compared to the WT control cells (Fig. 2B, 2C with IHD-J strain and Fig. S1C, S1D, S1E with Western Reserve strain of VV). Next, we tested replication of Herpes simplex virus-1 (HSV) and observed reduced viral replication at different multiplicity of infections (MOI) in OASL-KO BJ-Tert cells (Fig. 2D). We confirmed these observations in primary fibroblasts from *Oasl2*$^{-/-}$ mice with HSV and Mouse Cytomegalovirus (MCMV) infections (Fig. 2E and 2F). Similarly, OASL-KO cells showed reduced viral replication when infected with another dsDNA virus, Adenovirus (Adeno-GFP) (Fig. 2G and Fig. S1F). Taken together these observations validated our *in vivo* results and established that the loss of human *OASL* and mouse *Oasl2* reduces cellular permissiveness and increases cellular resistance to a variety of DNA virus infections.

OASL negatively regulates DNA virus-mediated IFN induction

We had previously shown that OASL neither affected IFN receptor or downstream signaling nor the ISG induction by IFN (Zhu et al., 2014). Therefore, to understand the observed

modulation of DNA virus replication by OASL, we investigated the changes in IFN induction after virus infection. VSV spreads to the CNS through the olfactory bulb when infected through the intranasal route (Detje et al., 2015). Thus, we measured IFN mRNA induction by reverse transcription coupled with quantitative PCR (RT-qPCR) in the olfactory bulbs of VSV infected mice. As expected, *in vivo* IFNα mRNA induction was reduced in the olfactory bulbs of VSVinfected *Oasl2*$^{-/-}$ mice compared to the WT mice (Fig. S2A) corroborating the protective role of *Oasl2* against RNA viruses. However, during intranasal infection of VV, the primary site of virus infection is the respiratory system (Goulding et al., 2012)(Fig. 1C). Therefore, we measured IFN induction in the cells harvested from bronchoalveolar lavage (BAL) of the infected mice. We found there was significant increased induction of IFNα in the total (Fig. 3A) as well as CD11c^{+} (Fig. S2B) cells from VV-infected *Oasl2*$^{-/-}$ mice compared to control WT mice. This indicated that although *Oasl2* enhances IFN induction during RNA virus infection and contributes to the host protection, during DNA virus infection it has an opposite function of negatively regulating IFN induction *in vivo*.

Next, we examined the role of *Oasl2* and *OASL* during IFN induction by DNA viruses *in vitro*. As shown in Fig. 3B (and Fig. S2C) IFNα, β and IFIT1 mRNA were significantly upregulated in OASL-KO BJ-Tert cells compared to the WT cells at two different does of VV. Similar trend was observed at the protein level of IFNβ (Fig. S2D). The enhanced IFN and ISG induction in OASL-KO cells were consistently observed during the late time points. We also used neutralizing antibody against IFN-receptor (IFNAR) to pretreat the OASL-KO cells followed by VV-Luc infection, which significantly, albeit not completely reversed the virus replication compared to the control antibody treated cells (Fig. S2E). This indicated that the reduced VV-Luc replication was caused by the enhanced IFN induction in the OASL-KO cells.

To examine the generalizability of the enhanced IFN induction in OASL-KO cells by other DNA virus infection we infected the same cells with HSV. As shown in Fig. 3C, OASL-KO BJ-tert cells expressed significantly higher level of IFNβ compared to the WT cells. In addition to WT HSV, which does not induce a robust IFN response due to the immuno-evasive activity of the viral immediate early genes, we also used a mutant variant d109 (HSV-d109) (Samaniego et al., 1998). In parallel experiments using increasing doses of an RNA virus (Sendai virus, SeV) and a DNA virus (HSV-d109) we observed the differential ability of *OASL* to influence IFN induction (Fig. S2G and Fig. 3D). Heightened IFNβ induction with HSV-d109 infection was observed in three different OASL-KO clones (Fig. S2H). We also saw the increased induction of ISG60 (IFIT3) in OASL-KO BJ-Tert cells at the protein level (Fig. S2I).

The delayed kinetics of the OASL-mediated inhibitory effect on IFN induction during VV infection led us to hypothesize that OASL might be acting as a feedback regulator of IFN induction. To examine this hypothesis, we measured the kinetics of OASL (in WT BJ-Tert cells), and IFNβ mRNA induction in WT and OASL-KO BJ-Tert cells following HSV-d109 infection. As shown in Fig. 3E, there was significantly higher IFNβ mRNA induction in OASL-KO cells at 48 h post-infection (hpi), while OASL mRNA was strongly induced earlier at 24 hpi in WT cells. This kinetics suggested a negative feedback regulation of IFN

induction by OASL. To further explore the broader effects of OASL we carried out transcriptomic analysis of the WT and OASL-KO BJ-Tert cells following DNA virus infection. Cells were infected with HSV-d109 at 2 MOI for 24 and 48 h followed by the RNA sequencing analysis. As shown in Fig. 3F a large number of genes, primarily ISGs, were induced at higher levels at 48 h in OASL-KO cells compared to the WT cells corroborating our qRT-PCR results.

Finally, we used exogenous OASL expression to further validate the observed effect of OASL on IFN induction by DNA virus infection. Vector control or OASL-expressing BJ-Tert cells (Fig. S2J) were infected with different doses of HSV-d109 followed by the detection of IFNβ protein in the culture supernatants. Consistent with our results from *OASL*-deficient cells, the ectopic expression of OASL significantly reduced IFNβ production by HSV-d109 infected cells (Fig. 3G). The results described here indicate that OASL acts as an inhibitor of the DNA virus mediated IFN induction. As a result, in the absence of OASL, IFN and ISG induction is enhanced after DNA virus infection effectively reducing virus replication. Kinetically, the suppressive effect of OASL on IFN induction appears to indicate a negative feedback regulation of IFN induction by OASL.

OASL inhibits cGAS-mediated IFN induction

Next, we investigated whether the inhibitory effect of OASL on IFN induction during DNA virus infection is a generalized inhibition of the cGAS-STING DNA-sensor signaling by OASL. Vector control and OASL-expressing THP1 cells were transfected with 100 bp dsDNA. As shown in Fig. 4A the presence of OASL significantly inhibited IFNβ protein production by dsDNA at various post-treatment time points. As expected, loss of OASL did not affect TLR3 signaling and negatively affected RIG-I signaling (Fig. S3A). Furthermore, to exclude the possibility of the off-target effects of CRISPR-Cas9-mediated genome editing, we transduced the OASL-KO BJ-tert cells with lentivirus expressing OASL and examined their response to dsDNA stimulation. Two separate pools of cells transduced with OASL-expressing lentivirus showed expected reduction in IFNβ induction establishing the negative regulatory role of OASL on DNA-sensing (Fig. 4B).

Having established the negative regulation of DNA-mediated IFN induction by OASL, we investigated the specific step/s of the cGAS-STING signaling pathway that was affected by OASL. In the context of RNA virus infection, we had shown that OASL enhanced RIG-I signaling, but this stimulatory effect of OASL was absent when the signaling pathway was activated by the overexpression of downstream components such as, MAVS, TBK1 or constitutively active IRF3 (Zhu et al., 2014). This indicated that OASL affected RIG-I but did not affect TBK1 and IRF3 mediated downstream signaling. However, to examine the effect of OASL on IRF3 activation downstream of cGAS-STING signaling we measured IRF3 phosphorylation. WT or OASL-KO BJ-Tert cells were treated with IFNα to induce OASL followed by dsDNA stimulation (Fig. 4C). Compared to the WT cells, OASL-KO cells exhibited enhanced IRF3 phosphorylation indicating that OASL affected the signaling pathway upstream of IRF3. Thus, we hypothesized that OASL might regulate either cGAS or STING activation. We examined this hypothesis by stimulating WT and OASL-KO THP1 cells (Fig. S3B) either with cGAS-ligand dsDNA (100 bp), or STING-ligand cGAMP. As

shown in Fig. 4D, OASL-KO THP1 cells when transfected with dsDNA showed increased IFNβ mRNA induction compared to the WT cells. However, when the same cells were transfected with cGAMP no difference in IFNβ mRNA induction was observed between two cell types (Fig. 4D). This result indicated that OASL-mediated inhibition of the cGAS-STING pathway occurred upstream of STING and most likely affected cGAS. These results were further confirmed in BJ-Tert cells. For this experiment, BJ-Tert cells were subjected to mild detergent permeabilization followed by cGAMP treatment as a strategy to activate STING (Woodward et al., 2010). Here again, OASL-KO cells did not show any difference in cGAMP-mediated ISG60 induction compared to the WT cells (Fig. 4E). Besides dsDNA transfection, we also used overexpression of cGAS and STING to induce ISG. In this system, the loss of OASL enhanced only dsDNA or cGAS overexpression mediated ISG60 induction without affecting STING overexpression mediated ISG60 induction (Fig. S3C). These results confirmed that OASL did not affect IFN induction mediated by STING activation and had no detectable effect on subsequent ISG induction.

To further corroborate these results in the context of virus infection, we generated cGASdeficient BJ-Tert cells (cGAS-KO) using CRISPR/Cas9 genome editing (Fig. S3D). As expected, cGAS-KO cells were severely defective in dsDNA-mediated ISG60 induction, but induced ISG60 upon stimulation with p(I):p(C) (Fig. S3E). Concomitantly, infection of these cGAS-KO cells with VV-Luc resulted in increased VV replication compared to the WT cells [Fig. 4F, compare WT-control (filled circles) vs. cGAS-KO control (open circles)]. As expected, expression of OASL caused a significant increase in virus replication in WT cells [Fig. 4F, compare WT-control (closed circles) with WT-OASL (closed squares)]; however similar expression of OASL (Fig. 4F inset) did not affect VV replication in cGAS-KO cells [Fig. 4F, compare cGAS-control (open circles) with cGAS-OASL (open squares)]. Similar results were obtained with a lower dose of VV (Fig. S3F). Furthermore, the loss of OASL did not significantly reduce VV replication in cGAS-OASL double-deficient cells compared to the only cGAS-deficient cells (Fig. S3G and S3H). These results indicate that the effect of OASL on VV replication is through cGAS and the loss of cGAS abolishes this effect. Taken together these findings suggest that OASL inhibits cGAS-mediated IFN induction resulting in enhanced replication of DNA viruses.

OASL interacts with cGAS

Next, we sought to determine the mechanism underlying OASL-mediated cGAS inhibition. As both the molecules are closely related, we first investigated whether OASL physically interacted with cGAS to modulate its function. V5-tagged OASL with FLAG-tagged cGAS were cotransfected in HEK293 cells followed by immunoprecipitation of cGAS using FLAG antibody (Fig. 5A). In this assay OASL specifically co-immunoprecipitated with cGAS, while another OAS-family member OAS1 did not (Fig. 5A). In a similar experiment OASL was immunoprecipitated with V5-antibody, cGAS (RIG-I was used as a positive control, (Zhu et al., 2014)) co-immunoprecipitated with OASL, while similarly tagged TRAF6 did not (Fig. 5B). Reverse immunoprecipitation of the same lysates further validated OASL-cGAS interaction (Fig. S4A). The endogenous OASL and cGAS interaction was established in IFNα-treated HeLa cells. As expected OASL was induced after IFNα stimulation and immunoprecipitated with cGAS only when it was induced by IFNα (Fig. 5C). The

physiological relevance of OASL-cGAS interaction was corroborated through immunofluorescence studies (Fig. 5D). OASL-V5 expressing HeLa cells were transfected with dsDNA. Although OASL partially colocalized with cGAS in untransfected cells (Fig. 5D bottom panel), following dsDNA transfection cGAS and OASL colocalized in characteristic puncta structures (Fig. 5D top panel) that are known to form upon cGAS activation (Collins et al., 2015).

Next, we determined the requirement of various domains of OASL for cGAS interaction using the same assay as before. Both full-length OASL and the C-terminal ubiquitin-like domain (UBL) deleted OASL (OASL-ΔUBL) interacted equally well with cGAS (Fig. 5E). In the same experiment, we also included DNase treated samples to examine the requirement of cellular DNA. Both full-length OASL and OASL-ΔUBL interacted with cGAS equally well irrespective of DNase treatments (Fig. 5E). In the context of OASL-mediated enhancement of RIG-I signaling the UBL domain of OASL was essential (Zhu et al., 2014). Since OASL-ΔUBL had similar interaction with cGAS compared to the full-length OASL, we examined the functional ability of OASL-ΔUBL to inhibit cGAS-mediated IFN induction using OASL-ΔUBL expressing cells (Fig. S4B). As shown in Fig. 5F, OASL-ΔUBL exhibited strong inhibition of IFN production when stimulated by dsDNA. This indicated that unlike the RNA-sensing pathway, modulation of the DNA sensing pathway by OASL did not require its UBL domain. We finally used a cell-free binding assay to examine the interaction of cGAS and OASL. As shown in Fig. 5G purified OASL and cGAS (Fig. S5A and S5B) were used in a Ni-NTA pull-down assay where equal quantities of OASL were pulled down with cGAS irrespective of dsDNA. Furthermore, we examined whether OASL affects DNA binding ability of cGAS using similar pull-down experiment using Biotin-labelled dsDNA. The presence of various concentrations of OASL did not seem to affect the amounts of cGAS pulled down by dsDNA indicating that OASL-binding did not impair the DNA-binding ability of cGAS (Fig. S5C). Following dsDNA binding, cGAS is suggested to form aggregates (Andreeva et al., 2017; Du and Chen, 2018; Hornung et al., 2014). We reasoned that OASL might bind to cGAS monomer thereby inhibit its dsDNA-mediated oligomerization. We tested this hypothesis using immunofluorescence microscopy to visualize the cGAS puncta formation resulting from cGAS aggregation (Banerjee et al., 2018; Collins et al., 2015). However, consistent with our previous result that OASL did not affect the DNA binding ability of cGAS, there was no significant difference in cGAS puncta formation between WT and OASL-KO BJ-tert cells after dsDNA stimulation (Fig. S5D). Together these results suggest that OASL interacts with cGAS and this interaction is independent of the presence of DNA.

OASL inhibits cGAMP production by cGAS

The above results suggest that OASL inhibited DNA virus-mediated IFN induction by interacting with cGAS. To define the molecular basis of OASL-mediated inhibition cGAS function we examined cGAMP production by cGAS in cells (Fig. 6A) and in solution (Fig. 6B-6D). Control WT and OASL-KO THP1 cells were transfected with dsDNA for 16 h followed by cGAMP quantitation in the cell extract by mass spectrometry. As shown in Fig. 6A cGAMP produced by the OASL-KO THP1 cells upon dsDNA stimulation was significantly higher than that by the WT cells. This result indicated that the presence of

OASL resulted in reduced cGAS activity in cells. To further confirm this result, we used cGAS activity assay using purified cGAS and OASL proteins (Fig. S5A and S5B). The production cGAMP by cGAS was inhibited by the presence of purified OASL in the reaction mixture in a concentration-dependent manner with an IC50 of 0.38 molar ratio of OASL:cGAS (Fig. 6B). Next, to determine the nature of this inhibition we carried out enzyme inhibition kinetics experiments with two cGAS substrates ATP (Fig. 6C) and GTP (Fig. 6D) over a range of substrate concentrations. Upon fitting the kinetic data with a Mixed-model inhibition (Copeland, 2005), the α in both cases turned out to be within 2–3, which indicated a non-competitive mode of inhibition. In summary, the cGAS activity assays described above strongly suggest that a physical interaction between cGAS and OASL results in the inhibition of cGAMP production by cGAS without affecting its DNA binding abilities.

DISCUSSION

Cellular IFN induction in response to virus infection is an essential process initiating the host inflammatory response to protect the host and clear virus infection. However, a negative regulatory mechanism is essential to inhibit the inflammation due to IFN response. Through the induction of hundreds of ISGs, IFN not only helps inhibit viral replication but also self-regulate to maintain tissue homeostasis (Schneider et al., 2014). Results from high-throughput screening assays for the antiviral activities of ISGs (Liu et al., 2012; Schoggins et al., 2011, 2014) have indicated that the antiviral activity of individual ISGs is variable depending on the virus and cell type used. Besides, there are species-specific discrepancies in ISG function (Busnadiego et al., 2014; Daugherty et al., 2016). Here, we describe a possible mechanistic basis for this virusspecific differential behavior of an individual ISG, OASL. We provide a mechanism for how OASL can work differently in a single cell in a context-dependent manner. Previously, we described a model for the antiviral activity of human OASL, where OASL binding to RIG-I enhanced RIG-I-mediated antiviral signaling to inhibit replication of RNA viruses (Zhu et al., 2014). Here we show that the same OASL can also bind to cGAS and inhibit cGAS activity to reduce IFN induction during DNA virus infection. A different mechanism for the negative regulatory role of mouse *Oasl1* on the IFN induction has been described before (Lee et al., 2013). However, here, we report the negative regulatory role of human *OASL* and mouse *Oasl2* – the functional homolog of *OASL*. Although differential effects of proteins have been reported before, in many cases the differential functions have been attributed to the differential expression of proteins in different cell types. Here we show that the same protein can work in opposing ways on two related but different receptor signaling pathways in the same cell.

The differential effect of OASL in the context of RNA and DNA sensor signaling has a structural basis. The UBL domain of OASL is essential for enhancing RIG-I activation and IFN induction. Mechanistically the UBL domain mimics K63-linked ubiquitin and promotes RIG-I activation. The same domain is also targeted by RNA viruses in order to evade IFN response providing evidence for its biological significance in the context of RNA virus infection (Dhar et al., 2015). In contrast, the UBL domain of OASL does not seem to be essential for either binding or inhibition of cGAS. This brings up an interesting possibility regarding the effect of OASL on RNA virus infections, which are also affected by cGAS-

STING pathway beside RLR pathway. For example, cGAS-STING-mediated IFN induction has been implicated in DENV (Aguirre and Fernandez-Sesma, 2017) and WNV replication (Schoggins et al., 2014). In fact, NS5 protein from DENV targets STING and cGAS to evade the IFN response initiated through DNA-sensor pathway (Aguirre and Fernandez-Sesma, 2017). In this context, it may be possible that RNA viruses have evolved strategies to target OASL and cleave the UBL domain to not only inhibit RIG-I signaling, but to promote additional inhibition of cGAS signaling through the remaining OAS domain.

The biological significance of the cytoplasmic DNA sensing through the cGAS-STING pathway goes beyond antiviral innate immunity. Recent studies have shown that a number of essential cellular processes are affected by this pathway including cellular senescence, telomere length maintenance and DNA-damage response (Chen et al., 2017b; Glück et al., 2017; Harding et al., 2017; Yang et al., 2017). Therefore, negative regulation of this pathway is essential for the cellular homeostasis. Furthermore, given that cGAMP itself can propagate from cell-to-cell spreading inflammatory signal, it is necessary to inhibit cGAS activity during chronic inflammatory condition. Although a few mechanisms have been described for the negative regulation of the cGAS-STING pathway, the majority of them involve the inhibition of STINGmediated signal transduction (Chen et al., 2016; Guo et al., 2016; Hu et al., 2016; Konno et al., 2013; Liang et al., 2014; Zhang et al., 2014). In this context, OASL is a direct inhibitor of cGAS enzyme activity that is described here. Furthermore, as OASL is inducible downstream of IRF3, it works as an effective negative-feedback regulator of the cGAS signaling at the later phase of the virus infection to control inflammation. While our manuscript was in final revision Lum *et al* found OASL as one of the cGAS interacting proteins through a proteomic screen and reported inhibition of cGAS-mediated IFNβ induction by OASL (Lum et al., 2018). This finding further confirms our results.

An important question arising from our finding is why OASL evolved to provide such differential activity against DNA versus RNA viruses? The answer might lie in the difference of duration and pathogenicity between the DNA and RNA viruses. Besides retroviruses, a majority of RNA viruses cause acute infection with shorter duration followed by clearance. In this context, IFN-mediated inflammation is beneficial to the host for initial suppression of viral replication and later viral clearance. On the contrary, the majority of DNA viruses causes chronic and life-long infections, resulting in persistence or latency depending on the virus. Therefore, it might be important for the host to restrict chronic inflammation through DNA sensing and IFN induction when infected with a DNA virus. It may also be important in the context of bacterial infection where cGAS-STING-mediated IFN induction might be deleterious for the host (Auerbuch et al., 2004; Mayer-Barber et al., 2014; McNab et al., 2015). Furthermore, cGASSTING pathway mediated IFN induction is important for the development of autoimmune diseases (Crow, 2016; Crow and Manel, 2015; Crowl et al., 2017). Our results, therefore, would predict that a loss of OASL might render the host more susceptible to autoimmunity. Indeed there are reports in the literature regarding an association of OASL with autoimmune diseases, although the mechanism remains unclear (Choi et al., 2015; Ye et al., 2006). In summary, our study identifies a protein inhibitor of cGAS and describes how this protein differentially regulates DNA- and RNA-sensor signaling.

STAR METHODS

CONTACT FOR REAGENT AND RESOURCE SHARING

Further information and requests for resources and reagents should be directed to and will be fulfilled by the Lead Contact, Saumendra N. Sarkar (saumen@pitt.edu).

EXPERIMENTAL MODEL AND SUBJECT DETAILS

Mice—All mice experiments were carried out according to the protocol approved by the University of Pittsburgh IACUC committee. WT and *Oasl2*$^{-/-}$ mice both in C57BL/6N background have been described before (Zhu et al., 2014). All mice were maintained in a pathogen-free facility. Virus infection experiments were carried out in approximately equal proportion of male and female

Cells and viruses—HEK293 (Source: Human embryonic kidney, Age/Sex: unknown), Vero (Source: African green monkey kidney, Age/Sex: unknown), BSC-1 (Source: African green monkey, Age/Sex: unknown), BJ-Tert (also called BJ-5ta, Source: Human foreskin, Age/Sex: neonatal male) and THP1 (Source: Human acute monocytic leukemia, Age/Sex: 1 year male) cells were obtained from ATCC. The specific HeLa cell line (also called HeLa LT) were obtained from the laboratory of Dr. Roderick J. O'Sullivan as described in (O'Sullivan et al., 2014). We found these cells express both cGAS and STING and are capable of inducing IFN and ISG by dsDNA transfection. Cell lines were checked monthly for mycoplasma contamination by DAPI staining and commercial PCR (Roche Diagnostics).

SeV, GFP tagged VSV and HSV-1 have been described before (Zhu et al., 2014). EGFP-labelled Adenovirus was a gift from Dr. Andrea Gambotto (University of Pittsburgh) and described in (Tüting et al., 1999). HSV-d109 has been described previously (Samaniego et al., 1998). GFP-tagged MCMV (K181 strain) was a gift from Dr. Chris Benedict (La Jolla Institute for Allergy and Immunology)(Horan et al., 2013) and amplified in NIH3T3 cells. Luciferase-tagged VV (IHD-J and Western Reserve strains) have been described before (Kirn et al., 2007; Reeves et al., 2011).

METHOD DETAILS

Cell line generation and stimulation—All the cell lines except THP1 were maintained in DMEM (Lonza, Rockland, ME) supplemented with 10% FBS (Atlanta Biologicals, Lawrenceville, GA) and Penicillin/Streptomycin. THP1 cells were maintained in RPMI (Lonza, Rockland, ME) supplemented with 10% FBS and Penicillin/Streptomycin. CRISPR-Cas9-mediated genome editing to generate OASL, cGAS deficient BJ-Tert and THP1 cells have been described before (Schmidt et al., 2016; Zhu et al., 2014). Briefly, plasmids carrying Cas9-mCherry and gRNA expression cassettes were transiently transfected to the respective cell lines followed by single-cell sorting of mCherry positive cells in 96 well plates. Colonies grown from single cells were screened by western blotting to identify specific knockout clones. Knockout BJ-Tert and THP1 clones were further confirmed by sequencing the target region as described before (Schmid-Burgk et al., 2014; Schmidt et al., 2016). We used the same approach to generate cGAS and OASL singly deficient HeLa cells. cGAS-deficient HeLa cells were used as the starting cell line to generate OASL-cGAS

double deficient HeLa cells. All variants of HeLa cell lines were validated by immunoblotting. Mouse fibroblasts were obtained from respective strains of adult mice (4–6 weeks old) tails by dissociating small pieces of tissue with collagenase (1000 U/ml) and trypsin. Cells were transfected with cGAMP with Lipofectamine 3000, dsDNA and p(I:C) with Lipofectamine 2000 at indicated concentration according to manufacturer's instructions.

Virus Infections and quantitation—For *in vivo* VV infection 4–6 weeks old mice were anesthetized by isoflurane and inoculated with VV-Luc (IHD-J strain) 1×10^4 pfu/nostril in 25 μl. Virus spread in mice were measured by whole body imaging using IVIS 200 (Perkin Elmer) following intraperitoneal injection of D–luciferin (Goldbio, St. Louis, MO) (4.5 mg/mice). For VSV infection anesthetized mice were inoculated intranasally with 1×10^5 pfu/nostril VSV in PBS. Mice were monitored daily for weight loss and scored for signs of illness. At indicated times mice were sacrificed and the olfactory bulb, as well as the brain tissues were collected for further analysis. For IHC analysis, the organs were fixed in 4% formalin. Slides were prepared from paraffin embedded tissues and detected with anti-GFP antibody (Santa Cruz Biotechnology). For RNA extraction, frozen tissues were homogenized using a Teflon coated mortar and pestle in Trizol (Invitrogen). cDNA was prepared from 1 μg of total RNA and analyzed by RT-qPCR with specific primers. Plaque assays for different viruses were carried out in the following cells. VV (IHDJ and WR strains) on BSC1 cells, HSV1 (KOS) on Vero cells and MCMV on NIH 3T3 cells. In each case, supernatants from virus infected cells were collected and plated in triplicate on the monolayers of indicated cells following serial dilutions. Plaques were visualized after 4–5 days by staining the monolayers with 2% crystal violet and manually counted. VV-Luc replication was quantified by measuring bioluminescence in IVIS 200 after adding D–luciferin (150 μg/ml) on the infected cells.

Purification of recombinant protein: Purification of cGAS has been described before (Li et al., 2013b). Briefly, human cGAS catalytically active domain (amino acid 157–522) and human OASL were cloned into a modified pET-28(a) vector with an N-terminal SUMO tag. Protein expression was induced by treating *E. coli* (Rosetta™ 2(DE3)) carrying respective plasmid with 0.4 mM IPTG at 16°C for 20 hours. Cells were centrifuged at 4500 rpm for 10 minutes at 4°C and resuspended in lysis buffer (50 mM TrisCl, pH 7.5; 500 mM NaCl, 5 mM β-mercaptoethanol). Cells were sonicated and spun down at 16,000 rpm for 30 minutes, supernatants were collected and loaded onto Ni-NTA column for protein binding. Columns were washed with washing buffer (20 mM Tris-Cl, pH 7.5, 500 mM NaCl, 25 mM Imidazole, 5 mM β-mercaptoethanol) followed by elution with buffer (20 mM Tris Cl, pH 7.5; 500 mM NaCl, 250 mM Imidazole and 5 μM βME). Eluted proteins were concentrated to 2 ml. For SUMO protease treatment, proteins were diluted to 15 ml and incubated with protease at 4°C overnight and loaded onto Ni NTA column to purify the cleaved SUMO tag. The eluted proteins were further purified on a Superdex 200 column in running buffer (20 mM Tris-Cl pH 7.5, 500 mM NaCl and 5 mM β-mercaptoethanol). Fractions containing the desired purified proteins were pooled, concentrated and subsequently used for *in vitro* studies.

cGAS Activity assay: For activity assay, cGAS (0.1 μg/ml) with OASL buffer (20 mM Tris.Cl pH 7.0, 100 mM NaCl) or cGAS and OASL (0.1 μg/ml each) were preincubated for 15 minutes at room temperature. A second mix was prepared with 45 bp dsDNA (1 μM) and either varying ATP concentrations (0, 0.5, 5, 50, 500 μM) and fixed GTP (500 μM) or varying GTP concentrations (0, 0.5, 5, 50, 500 μM) and fixed ATP (500 μM) in 2X assay buffer (100 mM TrisCl, pH 7.0; 10 mM Magnesium Acetate; 20 mM KCl, 0.2 mg/ml BSA). For each sample, first and second mixes were combined and incubated for 3 hours at 37°C. Samples were analyzed by mass spectrometry as described below.

Liquid Chromatography-Mass Spectrometric Quantitation of cGAMP: 2',3'-cGAMP, and internal standard c-di-AMP were obtained from Invivogen (San Diego, CA), and dissolved in water to generate stock solution aliquots. Aqueous calibrator solutions were prepared at 50–2000 ng/ml. Ten μl of c-di-AMP (1000 ng/ml in water) was added to each 40 μl of sample or calibrator. Samples were transferred to vials, capped and placed into the autosampler (kept at 4 °C). Aliquots of 10 or 20 μl from each vial was injected onto the LC–MS/MS system (Agilent 1200 Autosampler and Binary pump (Wilmington, DE, USA) coupled to an ABI4000Q bench top mass spectrometer (MDS SCIEX, Concord, ON, Canada). The analytes were separated on a Phenomenex Luna Phenylhexyl column (3 μm, 50 × 2.0 mm) isocratically perfused with 0.1% formic acid in water at a flow rate of 0.6 ml/min for 3.5 minutes. Retention times were 2.5 min (cGAMP) and 2.0 min (c-di-AMP). The settings of the mass spectrometer were as follows: curtain gas 50, IS voltage 5000 V, probe temperature 600°C, GS1 40, GS2 40, declustering potential 80 V, and collision energy 45 V. Quadrupoles were set to unit resolution and dwell time of 100 ms. The MRM m/z transitions monitored for cGAMP and c-di-AMP were 675.5>506.0, and 659.0>524.0, respectively. The high-performance liquid chromatography (HPLC) system and mass spectrometer were controlled by Analyst software (version 1.6.2), and data was collected with the same software. Standard curves of analyte-to-IS ratio versus concentrations were fitted by linear regression with weighting by 1/y2, followed by back calculation of concentrations.

Quantitative RT–PCR analysis—Total RNA was isolated from transfected and/or stimulated cells by Trizol (Life Technologies), and cDNA was synthesized using iScript cDNA Synthesis Kit (Bio-Rad, Hercules, CA). One part ($1/20^{th}$) of the cDNA synthesized from 1 μg RNA was subjected to real-time PCR using Fast EvaGreen Supermix in a CFX96 Real Time System (Bio-Rad) according to the manufacturer's instructions. All PCR amplification was normalized to ribosomal protein L32 (RPL32); the primers for human ISG56, ISG60, IFN-β and RPL32 have been described before (Zhu et al., 2014). Primers were custom synthesized by Integrated DNA Technologies (Coralville, IA).

Co-immunoprecipitation and Western-blotting—One million cells in 6-well plate transfected and/or treated as indicated were lysed in lysis buffer (Triton-X 100 1%, HEPES (pH 7.4) 20mM, NaCl 150mM, $MgCl_2$ 1.5mM, EGTA 2mM, DTT 2mM, NaF 10mM, β-Glycerophosphate 12.5mM, Na_3VO_4 1mM, PMSF 1mM, and Protease Inhibitor). The cleared cell lysates were incubated at 4 °C with respective antibody plus protein A/G agarose beads or anti-FLAG beads overnight, washed five times with lysis buffer, and boiled

in 2 × SDS–PAGE loading buffer for elution. Cell lysates boiled in 1 × SDS–PAGE loading buffer and immunoprecipitated samples were subjected to SDS-PAGE electrophoresis. Following transfer, the blots were incubated with target antibody followed by appropriate HRPconjugated secondary antibody and visualized by ECL detection (GE Healthcare).

Immunofluorescence: HeLa cells were transduced with OASL-V5 expressing lentivirus as described before (Zhu et al., 2014). Following 72 h of transduction, cells were either mock transfected or transfected with 1 μg/ml dsDNA for 4 h in chamber slides. Cells were fixed with ice-cold methanol:ethanol (1:1) mixture followed by immunostaining with anti-V5 and anti cGAS antibodies.

Immunofluorescence imaging was done on an Olympus IX81 microscope outfitted with a XLight V2 Spinning Disk Confocal imaging system (89 North, Inc. Burlington, VT). Z-stack images were captured and deconvoluted with Olympus Cellsense software.

Immunohistochemistry: Deparaffinized tissue sections were incubated with mouse anti-GFP monoclonal antibody (Santa Cruz, CA) overnight followed by washing with PBS three times. The slides were incubated with goat anti-mouse IgG tagged with horseradish peroxidase (HRP) (Rockland, PA). Cell staining was performed with DAB substrate kit (Vector Laboratories). Slides were counterstained with hematoxylin. Immunohistological images were acquired by an Olympus AX70 microscope and captured by Olympus camera.

IFN quantification: Human IFNβ in the cellular supernatant was quantified using Verikine-HS Human Interferon Beta Serum ELISA kit according to manufacturer's instructions.

DNA binding assay: Purified cGAS or cGAS and OASL at different ratios were mixed with biotinylated DNA in PBS, incubated at 4°C for 1 hour with gently shaking. The protein-DNA mix were then incubated with Streptavidin-agarose in a volume of 250 μl of PBS for 2 hours at 4°C with gently shaking. The beads were washed with 500 μl of PBS for four times and mixed with SDS-PAGE loading dye, boiled and loaded on a gel. The protein binding was visualized by staining the gel with Coomassie blue stain.

RNAseq analysis: 2×10^6 BJ-Tert Wt or OASL-KO cells in 60-mm plates were infected with HSV-d109 at a MOI of 2 at room temperature for 1 hour with rocking every 10 minutes. Following infection, the inoculum was removed, the cells were washed, and fresh pre-warmed media was added. Infections were carried out for 24 and 48 h with control mock infected cells. RNA was isolated with the Ambion RNaqueous-4PCR kit following the included protocol.

The harvested RNA was prepared for sequencing following the Illumina TruSeq RNA Sample Preparation v2 Guide and accompanying kit (Illumina, San Diego, CA). The libraries were analyzed for length and concentration using the Agilent Bioanalyzer. Samples for an experiment were mixed in equimolar concentration and sent to the Tufts University Sequencing Core Facility, Boston, MA, for sequencing. Sequencing was performed on an Illumina NextSeq 500. RNA-seq FASTQ data were processed and mapped to the human

reference genome (hg19) using CLC Genomics Workbench 11 (Qiagen). The RNAseq data from two biological replicates were used to determine HSV-d109 induced genes (log2-fold induction ≥ 2) at a significance cutoff of $P < 0.01$, followed by pairwise comparison between WT and OASL-KO samples at 48 h (fold change ≥ 1.2). Heat maps [based on RPKM values] were generated using pheatmap package in R.

QUANTIFICATION AND STATISTICAL ANALYSIS

Results shown are pooled samples from at least twice repeated for *in vivo* infection studies, and three times repeated for *in vitro* infection studies. For each data point mean and SEM were plotted, statistical significance were calculated either by two-way ANOVA with Sidak's multiple comparison test or by two-tailed Student's t-test as appropriate, and represented as * $P < 0.03$ and *** $P < 0.001$ using built in analysis function of GraphPad Prism 7.03.

ETOC BLURB AND HIGHLIGHTS

Etoc blurb—The interferon (IFN)-stimulated gene OASL enhances RNA sensor RIG-I-mediated IFN induction to inhibit RNA virus replication. In contrast, during DNA virus infection, Ghosh et al. show that OASL binds to the DNA sensor cGAS to inhibit interferon induction and enhance DNA virus replication. These findings highlight the distinct regulation of IFN induction by OASL during RNA and DNA virus infection.

Supplementary Material

Refer to Web version on PubMed Central for supplementary material.

ACKNOWLEDGMENTS

We are grateful to Dr. Andrea Gambotto, Dr. Chris Benedict and Dr. Veit Hornung for generously sharing crucial reagents. This work was supported in part by AI118896 and CA178766 from NIH. This project used a number of UPCI core facilities supported by P30CA047904.

REFERENCES

Ablasser A, Schmid-Burgk J, Hemmerling I, Horvath G, Schmidt T, Latz E, and Hornung V (2013). Cell intrinsic immunity spreads to bystander cells via the intercellular transfer of cGAMP. Nature 503, 530–534. [PubMed: 24077100]

Aguirre S, and Fernandez-Sesma A (2017). Collateral Damage during Dengue Virus Infection: Making Sense of DNA by cGAS. J. Virol 91, e01081–16.

Andreeva L, Hiller B, Kostrewa D, Lässig C, de Oliveira Mann CC, Jan Drexler D, Maiser A, Gaidt M, Leonhardt H, Hornung V, et al. (2017). cGAS senses long and HMGB/TFAM-bound U-turn DNA by forming protein–DNA ladders. Nature 549, 394–398. [PubMed: 28902841]

Auerbuch V, Brockstedt DG, Meyer-Morse N, O'Riordan M, and Portnoy DA (2004). Mice lacking the type I interferon receptor are resistant to Listeria monocytogenes. J. Exp. Med 200, 527–533. [PubMed: 15302899]

Banerjee I, Behl B, Mendonca M, Shrivastava G, Russo AJ, Menoret A, Ghosh A, Vella AT, Vanaja SK, Sarkar SN, et al. (2018). Gasdermin D Restrains Type I Interferon Response to Cytosolic DNA by Disrupting Ionic Homeostasis. Immunity 49, 413–426.e5. [PubMed: 30170814]

Busnadiego I, Kane M, Rihn SJ, Preugschas HF, Hughes J, Blanco-Melo D, Strouvelle VP, Zang TM, Willett BJ, Boutell C, et al. (2014). Host and Viral Determinants of Mx2 Antiretroviral Activity. J. Virol 88, 7738–7752. [PubMed: 24760893]

Chen Q, Sun L, and Chen ZJ (2016). Regulation and function of the cGAS-STING pathway of cytosolic DNA sensing. Nat. Immunol 17, 1142–1149. [PubMed: 27648547]

Chen S, Zhang W, Wu Z, Zhang J, Wang M, Jia R, Zhu D, Liu M, Sun K, Yang Q, et al. (2017a). Goose Mx and OASL Play Vital Roles in the Antiviral Effects of Type I, II, and III Interferon against Newly Emerging Avian Flavivirus. Front. Immunol 8, 1006. [PubMed: 28878774]

Chen Y-A, Shen Y-L, Hsia H-Y, Tiang Y-P, Sung T-L, and Chen L-Y (2017b). Extrachromosomal telomere repeat DNA is linked to ALT development via cGAS-STING DNA sensing pathway. Nat. Struct. Mol. Biol 24, 1124–1131. [PubMed: 29106411]

Choi UY, Kang J-S, Hwang YS, and Kim Y-J (2015). Oligoadenylate synthase-like (OASL) proteins: dual functions and associations with diseases. Exp. Mol. Med 47, e144. [PubMed: 25744296]

Civril F, Deimling T, de Oliveira Mann CC, Ablasser A, Moldt M, Witte G, Hornung V, and Hopfner K-P (2013). Structural mechanism of cytosolic DNA sensing by cGAS. Nature 498, 332–337. [PubMed: 23722159]

Collins AC, Cai H, Li T, Franco LH, Li XD, Nair VR, Scharn CR, Stamm CE, Levine B, Chen ZJ, et al. (2015). Cyclic GMP-AMP Synthase Is an Innate Immune DNA Sensor for Mycobacterium tuberculosis. Cell Host Microbe 17, 820–828. [PubMed: 26048137]

Copeland RA (2005). Evaluation of enzyme inhibitors in drug discovery. A guide for medicinal chemists and pharmacologists. Methods Biochem. Anal 46, 1–265. [PubMed: 16350889]

Crow MK (2016). Autoimmunity: Interferon α or β: which is the culprit in autoimmune disease? Nat. Rev. Rheumatol 12, 439–440. [PubMed: 27411904]

Crow Y, and Manel N (2015). Aicardi-Goutieres syndrome and the type I interferonopathies. Nat. Rev. Immunol 15, 429–440. [PubMed: 26052098]

Crowl JT, Gray EE, Pestal K, Volkman HE, and Stetson DB (2017). Intracellular Nucleic Acid Detection in Autoimmunity. Annu. Rev. Immunol 35, 313–336. [PubMed: 28142323]

Daugherty MD, Schaller AM, Geballe AP, and Malik HS (2016). Evolution-guided functional analyses reveal diverse antiviral specificities encoded by IFIT1 genes in mammals. Elife 5, e14228. [PubMed: 27240734]

Detje CN, Lienenklaus S, Chhatbar C, Spanier J, Prajeeth CK, Soldner C, Tovey MG, Schlüter D, Weiss S, Stangel M, et al. (2015). Upon Intranasal Vesicular Stomatitis Virus Infection, Astrocytes in the Olfactory Bulb Are Important Interferon Beta Producers That Protect from Lethal Encephalitis. J. Virol 89, 2731–2738. [PubMed: 25540366]

Dhar J, Cuevas RA, Goswami R, Zhu J, Sarkar SN, and Barik S (2015). 2' −5' Oligoadenylate Synthetase-Like Inhibits Respiratory Syncytial Virus Replication and is Targeted by the Viral Nonstructural Protein 1. J Virol 89, 10115–10119. [PubMed: 26178980]

Diner EJ, Burdette DL, Wilson SC, Monroe KM, Kellenberger CA, Hyodo M, Hayakawa Y, Hammond MC, and Vance RE (2013). The innate immune DNA sensor cGAS produces a noncanonical cyclic dinucleotide that activates human STING. Cell Rep. 3, 1355–1361. [PubMed: 23707065]

Dou Z, Ghosh K, Vizioli MG, Zhu J, Sen P, Wangensteen KJ, Simithy J, Lan Y, Lin Y, Zhou Z, et al. (2017). Cytoplasmic chromatin triggers inflammation in senescence and cancer. Nature 550, 402–406. [PubMed: 28976970]

Du M, and Chen ZJ (2018). DNA-induced liquid phase condensation of cGAS activates innate immune signaling. Science 361, 704–709. [PubMed: 29976794]

Gao P, Ascano M, Wu Y, Barchet W, Gaffney B, Zillinger T, Serganov A, Liu Y, Jones R, Hartmann G, et al. (2013). Cyclic [G(2',5')pA(3',5')p] Is the Metazoan Second Messenger Produced by DNA-Activated Cyclic GMP-AMP Synthase. Cell 153, 1094–1107. [PubMed: 23647843]

Glück S, Guey B, Gulen MF, Wolter K, Kang T-W, Schmacke NA, Bridgeman A, Rehwinkel J, Zender L, and Ablasser A (2017). Innate immune sensing of cytosolic chromatin fragments through cGAS promotes senescence. Nat. Cell Biol. 19, 1061–1070. [PubMed: 28759028]

Goulding J, Bogue R, Tahiliani V, Croft M, and Salek-Ardakani S (2012). CD8 T Cells Are Essential for Recovery from a Respiratory Vaccinia Virus Infection. J. Immunol 189, 2432–2440. [PubMed: 22826318]

Guo H, König R, Deng M, Riess M, Mo J, Zhang L, Petrucelli A, Yoh SM, Barefoot B, Samo M, et al. (2016). NLRX1 Sequesters STING to Negatively Regulate the Interferon Response, Thereby

Facilitating the Replication of HIV-1 and DNA Viruses. Cell Host Microbe 19, 515–528. [PubMed: 27078069]

Harding SM, Benci JL, Irianto J, Discher DE, Minn AJ, and Greenberg RA (2017). Mitotic progression following DNA damage enables pattern recognition within micronuclei. Nature 548, 466–470. [PubMed: 28759889]

Hartmann G (2017). Nucleic Acid Immunity. Advances in Immunology 133, 121–169. [PubMed: 28215278]

Horan K, Hansen K, Jakobsen M, Holm C, Søby S, Unterholzner L, Thompson M, West J, Iversen M, Rasmussen S, et al. (2013). Proteasomal degradation of herpes simplex virus capsids in macrophages releases DNA to the cytosol for recognition by DNA sensors. J. Immunol 190, 2311–2319. [PubMed: 23345332]

Hornung V, Hartmann R, Ablasser A, and Hopfner K-P (2014). OAS proteins and cGAS: unifying concepts in sensing and responding to cytosolic nucleic acids. Nat. Rev. Immunol 14, 521–528. [PubMed: 25033909]

Hu M-M, Yang Q, Xie X-Q, Liao C-Y, Lin H, Liu T-T, Yin L, and Shu H-B (2016). Sumoylation Promotes the Stability of the DNA Sensor cGAS and the Adaptor STING to Regulate the Kinetics of Response to DNA Virus. Immunity 45, 555–569. [PubMed: 27637147]

Kirn DH, Wang Y, Le Boeuf F, Bell J, and Thorne SH (2007). Targeting of InterferonBeta to Produce a Specific, Multi-Mechanistic Oncolytic Vaccinia Virus. PLoS Med. 4, e353. [PubMed: 18162040]

Konno H, Konno K, and Barber G (2013). Cyclic Dinucleotides Trigger ULK1 (ATG1) Phosphorylation of STING to Prevent Sustained Innate Immune Signaling. Cell 155, 688–698. [PubMed: 24119841]

Kranzusch PJ, Wilson SC, Lee ASY, Berger JM, Doudna JA, and Vance RE (2015). Ancient Origin of cGAS-STING Reveals Mechanism of Universal 2’,3’ cGAMP Signaling. Mol. Cell 59, 891–903. [PubMed: 26300263]

Kristiansen H, Gad HH, Eskildsen-Larsen S, Despres P, and Hartmann R (2011). The Oligoadenylate Synthetase Family: An Ancient Protein Family with Multiple Antiviral Activities. J. Interf. Cytokine Res. 31, 41–47.

Lee MS, Kim B, Oh GT, and Kim YJ (2013). OASL1 inhibits translation of the type i interferon-regulating transcription factor IRF7. Nat. Immunol 14, 346–355. [PubMed: 23416614]

Li X-D, Wu J, Gao D, Wang H, Sun L, and Chen Z (2013a). Pivotal roles of cGAScGAMP signaling in antiviral defense and immune adjuvant effects. Science 341, 1390–1394. [PubMed: 23989956]

Li X, Shu C, Yi G, Chaton C, Shelton C, Diao J, Zuo X, Kao CC, Herr A, and Li P (2013b). Cyclic GMP-AMP Synthase Is Activated by Double-Stranded DNA-Induced Oligomerization. Immunity 39, 1019–1031. [PubMed: 24332030]

Li Y, Banerjee S, Wang Y, Goldstein SA, Dong B, Gaughan C, Silverman RH, and Weiss SR (2016). Activation of RNase L is dependent on OAS3 expression during infection with diverse human viruses. Proc. Natl. Acad. Sci. U. S. A 113, 2241–2246. [PubMed: 26858407]

Liang Q, Seo GJ, Choi YJ, Kwak M-J, Ge J, Rodgers MA, Shi M, Leslie BJ, Hopfner K-P, Ha T, et al. (2014). Crosstalk between the cGAS DNA sensor and Beclin-1 autophagy protein shapes innate antimicrobial immune responses. Cell Host Microbe 15, 228–238. [PubMed: 24528868]

Liu S-Y, Sanchez D, Aliyari R, Lu S, and Cheng G (2012). Systematic identification of type I and type II interferon-induced antiviral factors. Proc. Natl. Acad. Sci 109, 4239–4244. [PubMed: 22371602]

Lum KK, Song B, Federspiel JD, Diner BA, Howard T, and Cristea IM (2018). Interactome and Proteome Dynamics Uncover Immune Modulatory Associations of the Pathogen Sensing Factor cGAS. Cell Syst. 10.1016/j.cels.2018.10.010.

Mackenzie KJ, Carroll P, Martin C-A, Murina O, Fluteau A, Simpson DJ, Olova N, Sutcliffe H, Rainger JK, Leitch A, et al. (2017). cGAS surveillance of micronuclei links genome instability to innate immunity. Nature 548, 461–465. [PubMed: 28738408]

Mayer-Barber KD, Andrade BB, Oland SD, Amaral EP, Barber DL, Gonzales J, Derrick SC, Shi R, Kumar NP, Wei W, et al. (2014). Host-directed therapy of tuberculosis based on interleukin-1 and type I interferon crosstalk. Nature 511, 99–103. [PubMed: 24990750]

McNab F, Mayer-Barber K, Sher A, Wack A, and O’Garra A (2015). Type I interferons in infectious disease. Nat Rev Immunol 15, 87–103. [PubMed: 25614319]

Nair S, Michaelsen-Preusse K, Finsterbusch K, Stegemann-Koniszewski S, Bruder D, Grashoff M, Korte M, Köster M, Kalinke U, Hauser H, et al. (2014). Interferon Regulatory Factor-1 Protects from Fatal Neurotropic Infection with Vesicular Stomatitis Virus by Specific Inhibition of Viral Replication in Neurons. PLoS Pathog 10, e1003999. [PubMed: 24675692]

O'Sullivan RJ, Arnoult N, Lackner DH, Oganesian L, Haggblom C, Corpet A, Almouzni G, and Karlseder J (2014). Rapid induction of alternative lengthening of telomeres by depletion of the histone chaperone ASF1. Nat. Struct. Mol. Biol 21, 167–174. [PubMed: 24413054]

Oh JE, Lee MS, Kim Y-J, and Lee HK (2016). OASL1 deficiency promotes antiviral protection against genital herpes simplex virus type 2 infection by enhancing type I interferon production. Sci. Rep 6, 19089. [PubMed: 26750802]

Reeves PM, Smith SK, Olson VA, Thorne SH, Bornmann W, Damon IK, and Kalman D (2011). Variola and Monkeypox Viruses Utilize Conserved Mechanisms of Virion Motility and Release That Depend on Abl and Src Family Tyrosine Kinases. J. Virol 85, 21–31. [PubMed: 20962097]

Samaniego LA, Neiderhiser L, and DeLuca NA (1998). Persistence and expression of the herpes simplex virus genome in the absence of immediate-early proteins. J. Virol 72, 3307–3320. [PubMed: 9525658]

Schmid-Burgk JL, Schmidt T, Gaidt MM, Pelka K, Latz E, Ebert TS, and Hornung V (2014). OutKnocker: a web tool for rapid and simple genotyping of designer nuclease edited cell lines. Genome Res. 24, 1719–1723. [PubMed: 25186908]

Schmidt T, Schmid-Burgk JL, Ebert TS, Gaidt MM, and Hornung V (2016). Designer Nuclease-Mediated Generation of Knockout THP1 Cells. In Methods in Molecular Biology (Clifton, N.J.), pp. 261–272.

Schneider WM, Chevillotte MD, and Rice CM (2014). Interferon-Stimulated Genes: A Complex Web of Host Defenses. Annu. Rev. Immunol 32, 513–545. [PubMed: 24555472]

Schoggins J, Wilson S, Panis M, Murphy M, Jones C, Bieniasz P, and Rice C (2011). A diverse range of gene products are effectors of the type I interferon antiviral response. Nature 472, 481–485. [PubMed: 21478870]

Schoggins J, MacDuff D, Imanaka N, Gainey M, Shrestha B, Eitson J, Mar K, Richardson B, Ratushny A, Litvak V, et al. (2014). Pan-viral specificity of IFN-induced genes reveals new roles for cGAS in innate immunity. Nature 505, 691–695. [PubMed: 24284630]

Sun L, Wu J, Du F, Chen X, and Chen Z (2012). Cyclic GMP-AMP Synthase Is a Cytosolic DNA Sensor That Activates the Type I Interferon Pathway. Science 339, 786–791. [PubMed: 23258413]

Tüting T, Steitz J, Brück J, Gambotto A, Steinbrink K, DeLeo AB, Robbins P, Knop J, and Enk AH (1999). Dendritic cell-based genetic immunization in mice with a recombinant adenovirus encoding murine TRP2 induces effective anti-melanoma immunity. J. Gene Med. 1, 400–406. [PubMed: 10753065]

Woodward JJ, Iavarone AT, and Portnoy DA (2010). c-di-AMP secreted by intracellular Listeria monocytogenes activates a host type I interferon response. Science 328, 1703–1705. [PubMed: 20508090]

Xia P, Ye B, Wang S, Zhu X, Du Y, Xiong Z, Tian Y, and Fan Z (2016). Glutamylation of the DNA sensor cGAS regulates its binding and synthase activity in antiviral immunity. Nat. Immunol 17, 369–378. [PubMed: 26829768]

Yang H, Wang H, Ren J, Chen Q, and Chen ZJ (2017). cGAS is essential for cellular senescence. Proc. Natl. Acad. Sci. U. S. A 114, E4612–E4620. [PubMed: 28533362]

Ye S, Guo Q, Tang J, Yang C, Shen N, and Chen S (2006). Could 2′5′-oligoadenylate synthetase isoforms be biomarkers to differentiate between disease flare and infection in lupus patients? A pilot study. Clin. Rheumatol 26, 186–190. [PubMed: 16565890]

Zhang L, Mo J, Swanson KV, Wen H, Petrucelli A, Gregory SM, Zhang Z, Schneider M, Jiang Y, Fitzgerald KA, et al. (2014). NLRC3, a member of the NLR family of proteins, is a negative regulator of innate immune signaling induced by the DNA sensor STING. Immunity 40, 329–341. [PubMed: 24560620]

Zheng S, Zhu D, Lian X, Liu W, Cao R, and Chen P (2016). Porcine 2', 5'oligoadenylate synthetases inhibit Japanese encephalitis virus replication in vitro. J. Med. Virol 88, 760–768. [PubMed: 26437676]

Zhu J, Zhang Y, Ghosh A, Cuevas RA, Forero A, Dhar J, Ibsen MS, Schmid-Burgk JL, Schmidt T, Ganapathiraju MK, et al. (2014). Antiviral activity of human OASL protein is mediated by enhancing signaling of the RIG-I RNA sensor. Immunity 40, 936–948. [PubMed: 24931123]

Highlights

1. Loss of human OASL and mouse Oasl2 inhibits DNA virus infection.
2. OASL and Oasl2 inhibit cGAS-mediated IFN induction
3. OASL specifically binds to cGAS to inhibit cGAS enzyme activity.
4. OASL binds to cGAS independently of double-stranded DNA

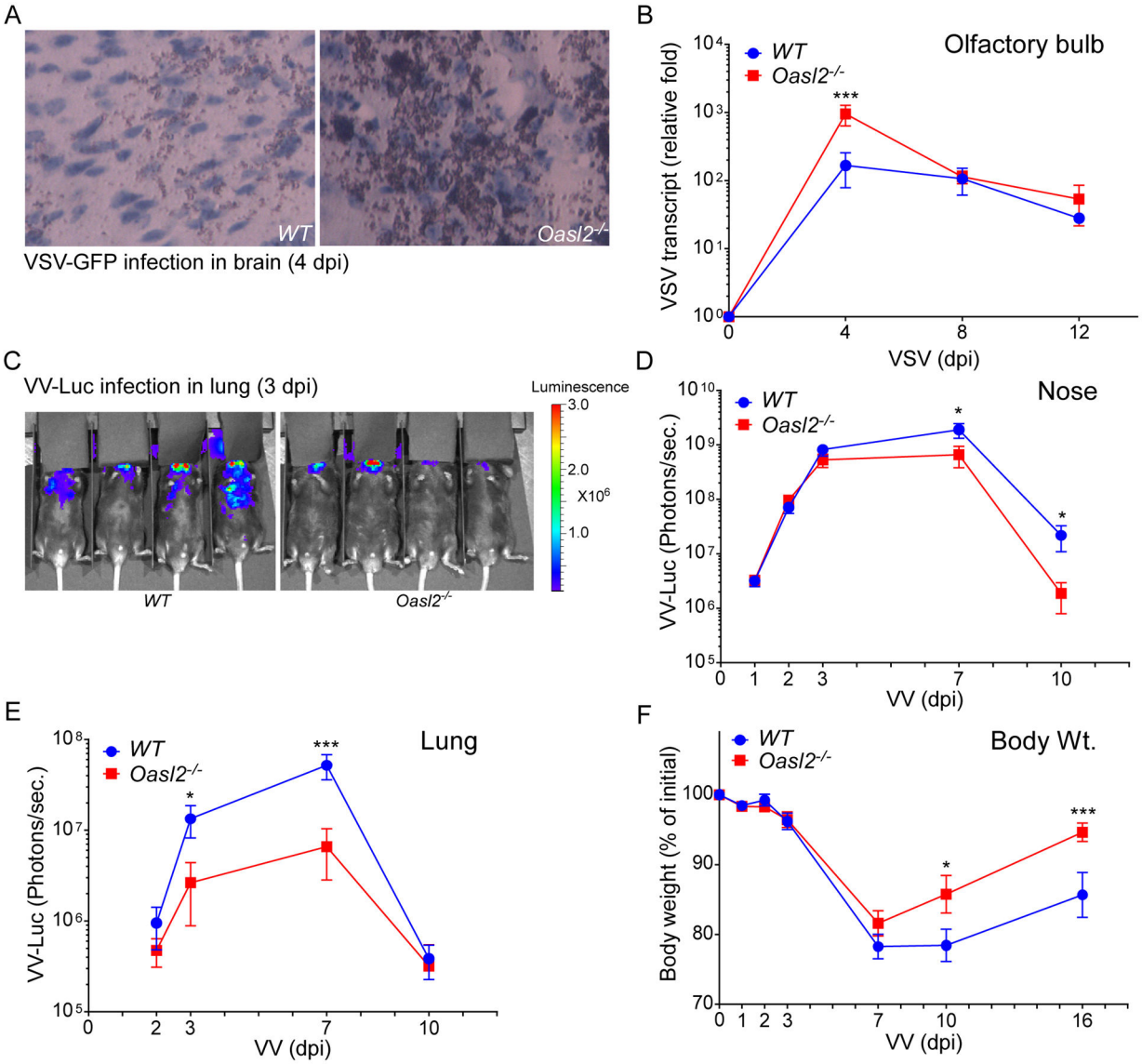

Fig. 1: RNA and DNA virus growth and pathogenesis in *Oasl2*$^{-/-}$ mice.

(A) Four to six weeks old WT and *Oasl2*$^{-/-}$ mice (N=9 each) were infected intranasally with VSV-GFP (2×10^5 pfu/mice). Representative immunohistochemistry of 4 days post-infection (dpi) mouse brain sections stained with GFP antibody are shown..

(B) Olfactory bulbs were harvested from WT and *Oasl2*$^{-/-}$ mice at indicated days. VSV transcripts were quantified from the tissue homogenate by RT-qPCR.

(C),(D) and (E) Four to six weeks old WT and *Oasl2*$^{-/-}$ mice (N=8 each) were infected intranasally with VV-Luc (2×10^4 pfu/mice). Virus replication and spread were quantified on indicated days by whole animal bioluminescence imaging.

(F) Losses of body weight of the mice infected as above were measured at indicated days postinfection.

Results shown are pooled samples from twice repeated *in vivo* infection studies. For each data point mean and SEM were plotted, statistical significances were calculated by two-way ANOVA with Sidak's multiple comparison test

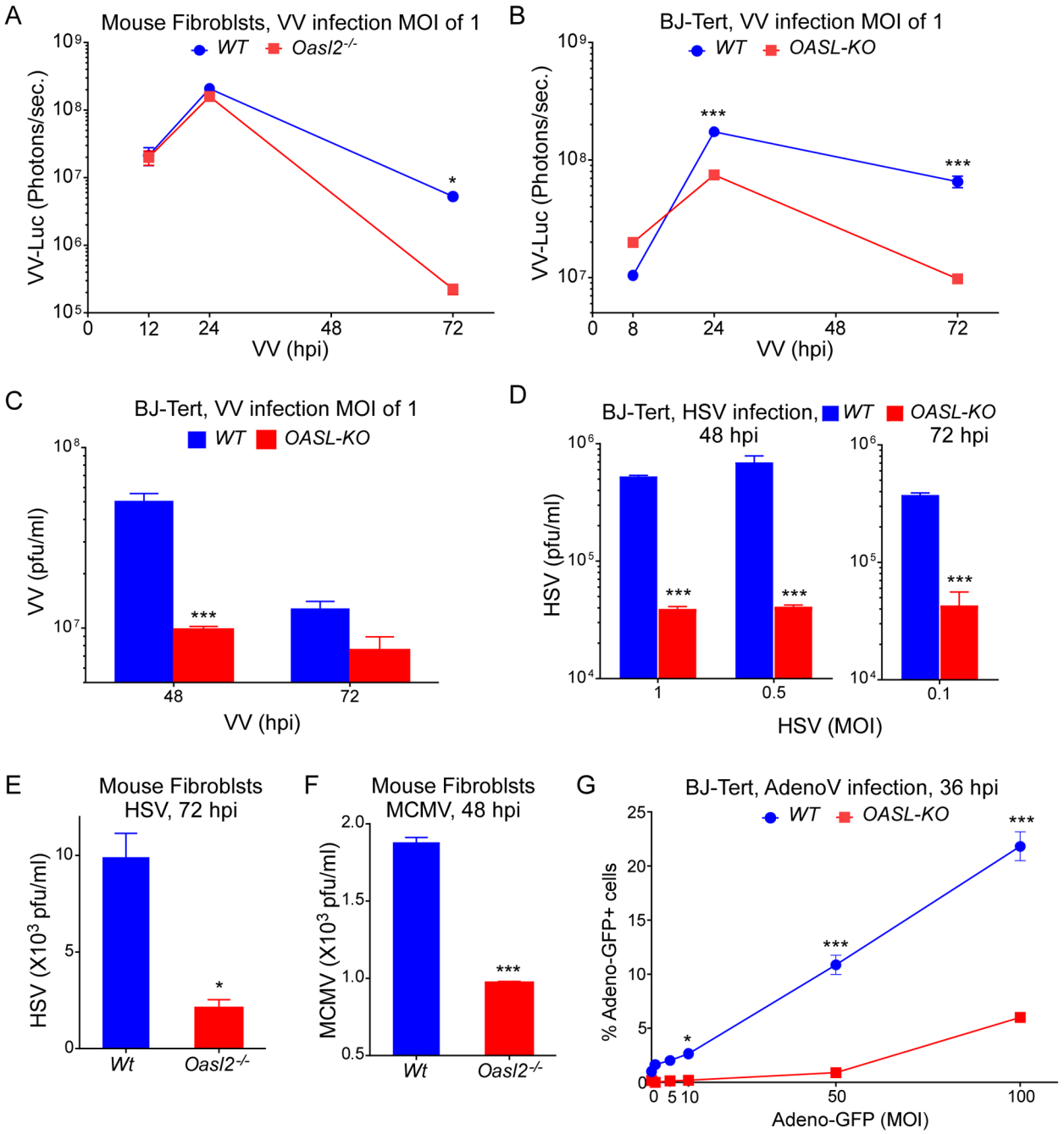

Fig. 2: Replication of multiple DNA viruses in OASL or Oasl2 deficient cells.

(A) and (B) Tail fibroblasts from WT and *Oasl2*$^{-/-}$ mice (A), and human BJ-Tert fibroblasts (B) were infected with VV-Luc (IHD-J strain) at MOI of 1. Virus replication was measured in triplicates at indicated times post-infection (hpi: hrs post-infection) by luciferase activity assay using IVIS200.

(C) WT and OASL-KO BJ-Tert cells were infected with VV as above. Infectious virus particles in the culture media were collected and quantified by plaque assay on BSC-1 cells.

(D)Equal numbers of WT and OASL-KO BJ-Tert cells were infected with HSV-1 at MOI of 1, 0.5 and 0.1. Culture supernatant were collected at 48 h (MOI of 1 and 0.5) and 72 h (MOI of 0.1) post-infection and infectious particles were quantified by plaque assay on Vero cells.
(E) and (F) Equal numbers of fibroblasts from WT and *Oasl2*$^{-/-}$ mice were infected with HSV at MOI of 0.1 for 72 h (E), and with MCMV at MOI of 0.1 for 48 h (F). Infectious particles in the culture supernatant were measured by plaque assay on Vero cells and NIH3T3 cells respectively.
(G) WT and OASL-KO BJ-Tert cells were infected with Adeno-GFP at MOI as indicated. Following 36 h of infection virus replication were quantified by measuring percentage of GFP+ cells by flow cytometry.
Results shown are pooled samples from three times repeated *in vitro* infection studies. For each data point mean and SEM were plotted. Statistical significance were calculated by two-way ANOVA with Sidak's multiple comparison test or by two-tailed Student's t-test (E and (F).

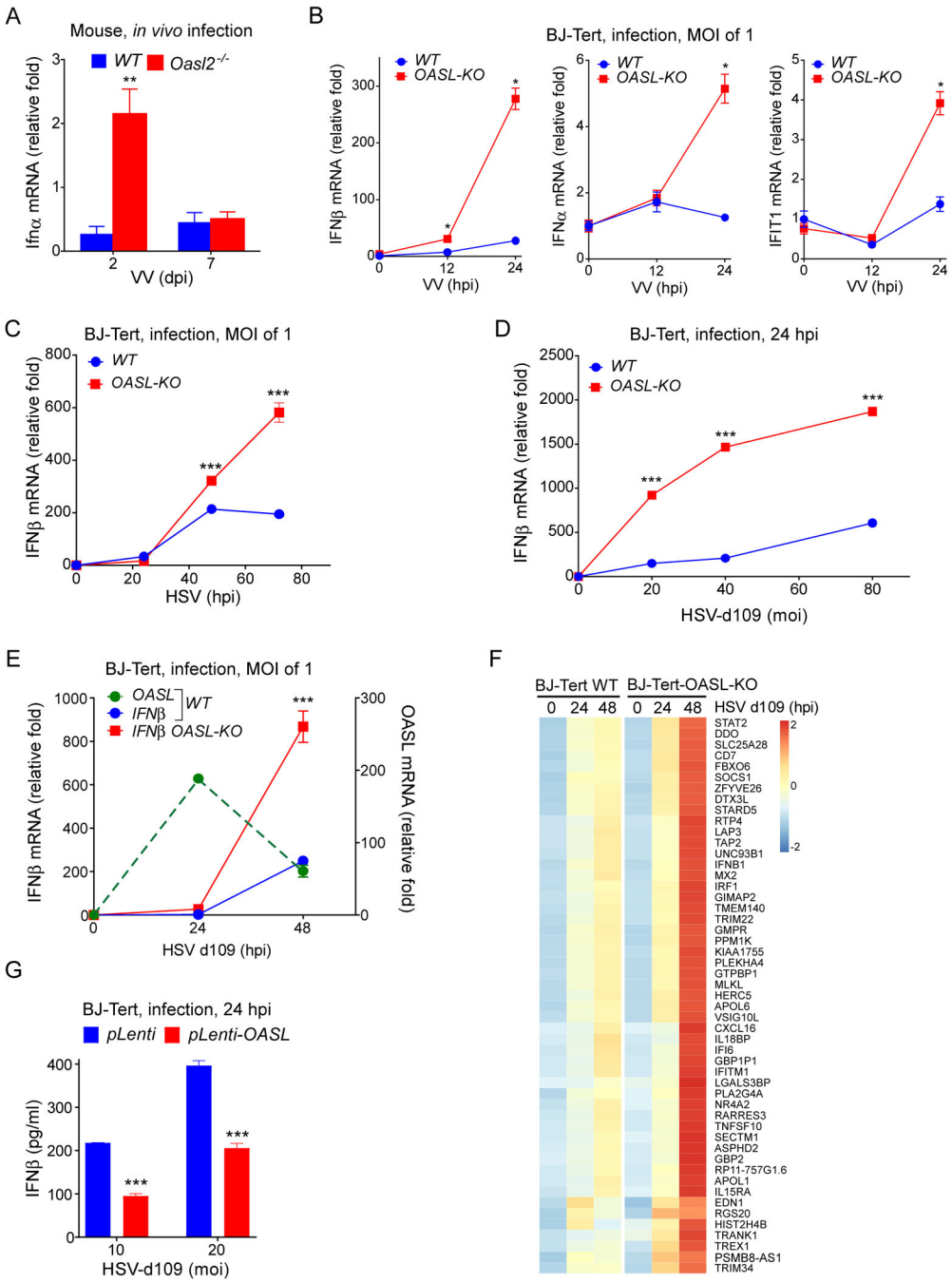

Fig. 3: Effect of OASL and Oasl2 on IFN induction by RNA and DNA viruses.

(A) WT and *Oasl2*$^{-/-}$ mice were infected with VV (IHD-J strain) as before (Fig. 1C). Mice were sacrificed as indicated followed by the collection of total cells from the BAL fluid of each mice, and quantitation of Ifnα mRNA by RT-qPCR.

(B) Equal numbers of WT and OASL-KO BJ-Tert cells were infected with VV at a MOI of 1. Total RNA was collected at 12 and 24 hpi, followed by the quantitation of IFNβ, IFNα and IFIT1 mRNA by RT-qPCR.

(C) Indicated cells were infected with HSV at MOI of 1. IFNβ mRNA induction was measured at different time points.
(D) WT and OASL-KO BJ-Tert cells were infected with HSV-d109 for 24 h with indicated doses followed by the analysis of IFNβ mRNA induction.
(E) Indicated cells were infected with HSV-d109 at MOI of 1 followed by the analysis of IFN03B2 and OASL mRNA induction by RT-qPCR.
(F) WT and OASL-KO BJ-Tert cells were infected with HSV-d109 at 2 MOI for the indicated times followed by the RNAseq analysis of the poly(A) containing transcriptome. Heatmap of a subset of genes that are significantly upregulated in OASL-KO cells is shown.
(G) BJ-Tert cells stably transduced with lentivirus carrying OASL or control vector were infected with HSV-d109 at MOI of 10 and 20 for 24 h. Culture supernatants were analyzed for IFNβ protein production after 24 h post-infection by ELISA.
Results shown are representative of at least three times repeated *in vitro* experiments (B) to (E) and (G). In panel (A), pooled samples from twice repeated *in vivo* infection studies were plotted, while the average values of twice repeated RNAseq experiments were used for the heatmap in (F).

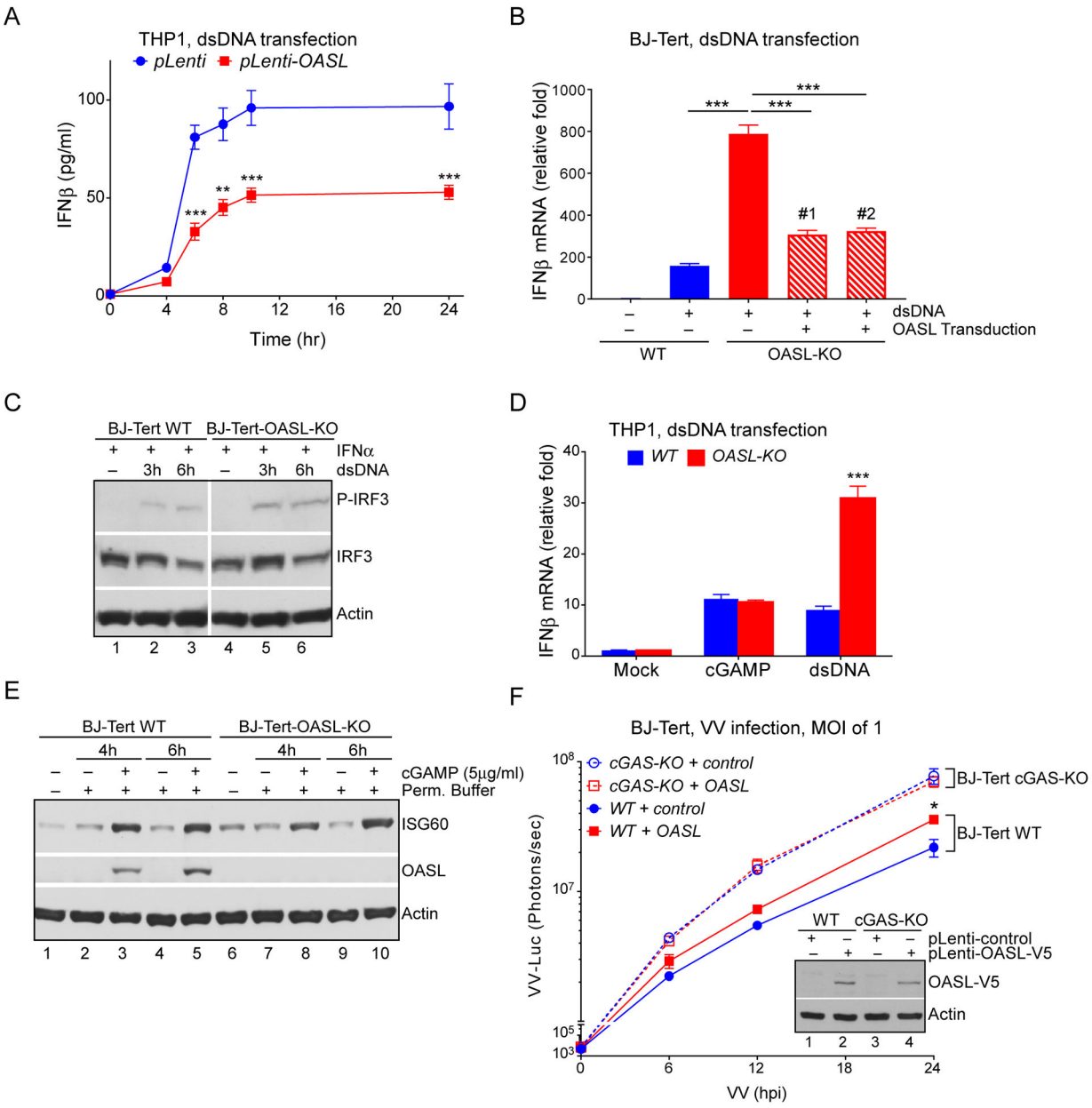

Fig. 4: Characterization of OASL effect on DNA-sensor signaling pathway.

(A) THP1 cells transduced similarly as before with OASL-expressing lentivirus were stimulated with dsDNA by transfection with 100 bp synthetic DNA (1 μg/ml) for the indicated times. Culture supernatants were analyzed for IFNβ protein production by ELISA.

(B) BJ-Tert OASL-KO cells were transduced with lentivirus carrying OASL followed by dsDNA transfection as indicated. IFNβ induction was measured by RT-qPCR.

(C) Indicated cells were treated overnight with 1000 U of IFNα to induce OASL followed by dsDNA transfection (100 bp synthetic DNA, 1 μg/ml) for the indicated times. Whole cell lysates were analyzed for IRF3 phosphorylation by immunoblotting with Phospho-IRF-3 (Ser396) antibody along with total IRF3 and Actin antibodies.

(D) WT and OASL-KO THP1 cells were stimulated either with dsDNA (100 bp synthetic DNA, 1 μg/ml) or with cGAMP (5 μg/ml) by transfection. IFNβ mRNA induction was analyzed after 6 h post-transfection by RT-qPCR.
(E) WT and OASL-KO BJ-Tert cells were permeabilized with Digitonin and treated with cGAMP (5 μg/ml) for 4 and 6 hrs as indicated. Cell lysates were immunoblotted with ISG60 (IFIT3), OASL and actin antibody.
(F) WT and cGAS-deficient (cGAS-KO) BJ-Tert cells were transduced with lentivirus carrying either OASL or the control vector and validated for protein expression by immunoblotting (inset). Cells were then infected with VV-Luc at MOI of 1 and the virus replication measured at indicated times by luciferase assays.
Results shown are representative of at least three times repeated *in vitro* experiments.

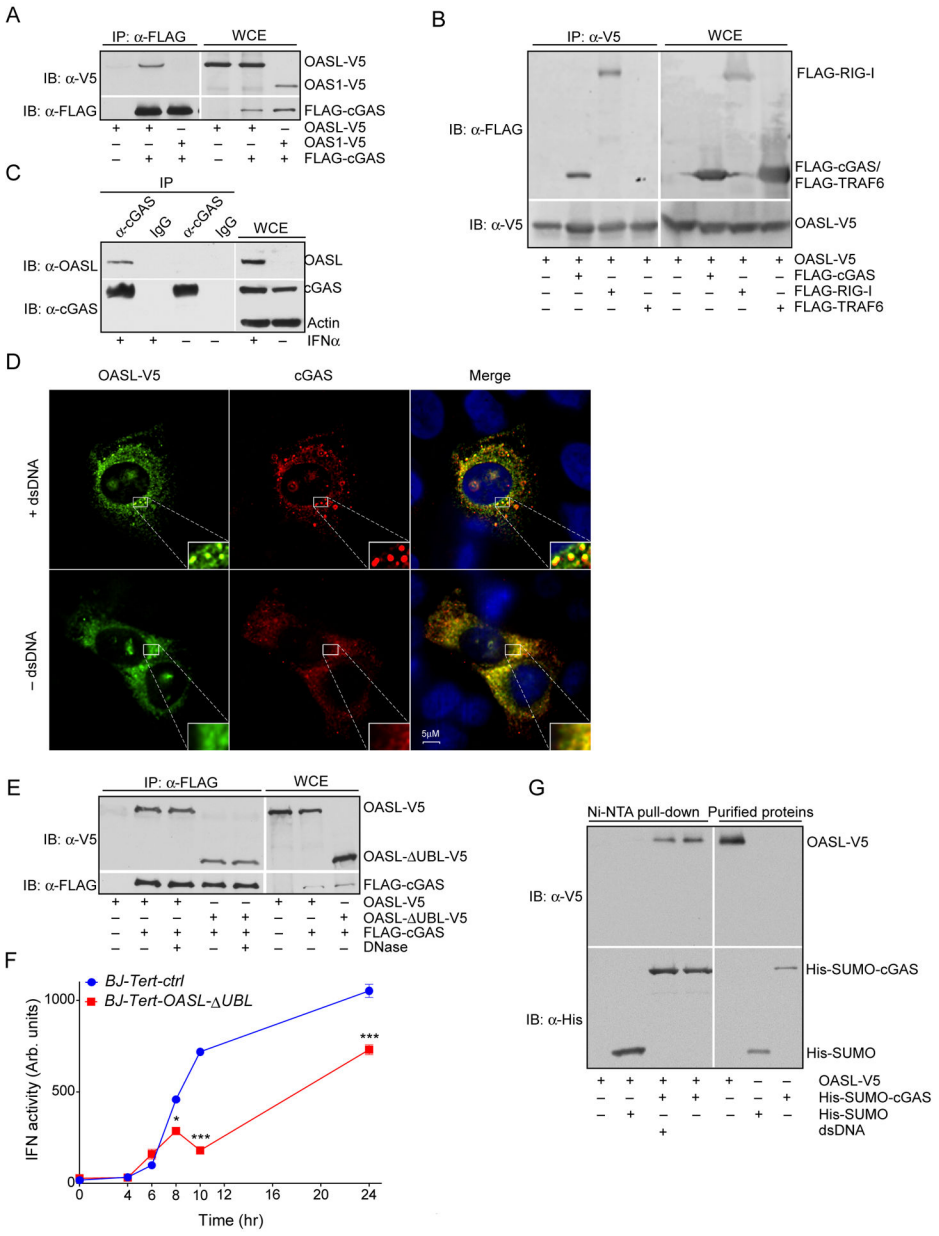

Fig. 5: Interaction of OASL and cGAS.

(A) C-terminal V5-tagged OASL (OASL-V5) or OAS1 (OAS1-V5) were cotransfected with Nterminal FLAG-tagged cGAS (FLAG-cGAS) in HEK293 cells for 24 h as indicated. Equal amounts of cell extracts (750 μg total protein) were immuneprecipitated (IP) with FLAG antibody (mouse monoclonal) followed by immunoblotting (IB) with either V5 (rabbit monoclonal) or FLAG (rabbit polyclonal) antibody. Whole cell lysates (WCE) were also immunoblotted in parallel to detect recombinant protein expression.

(B) Similarly, OASL-V5 was cotransfected either with FLAG-cGAS or FLAG-TRAF6 followed by IP with V5 (mouse monoclonal) antibody and IB with FLAG or V5 antibody.

(C) Control or IFNα treated HeLa cell extracts were immunoprecipitated either with cGAS antibody or control IgG followed by the detection of OASL with OASL antibody.

Concomitant immunoblotting of the whole cell lysate shows the respective protein expression.

(D) Immunofluorescence analysis of the OASL-V5 expressing HeLa cells with or without dsDNA transfection. HeLa cells stably transduced with OASL-V5 expressing lentivirus were stimulated with dsDNA by transfection for 4 h. Fixed cells were immunostained with cGAS and V5 antibodies followed by confocal microscopy. The insets show enlarged sections highlighting cGAS puncta formation after dsDNA stimulation. Scale bar = 5 μm.

(E) OASL-V5 or OASL-ΔUBL-V5 constructs were cotransfected with FLAG-cGAS as indicated in HEK293 cells followed by IP as above. Immunoprecipitated samples were resuspended in DNase reaction buffer with or without DNase I as indicated, incubated at room temperature for 15 minutes followed by washing and analysis by IB.

(F) BJ-Tert cells transduced with either control vector or OASL-ΔUBL-V5 carrying lentivirus were stimulated with dsDNA (100 bp synthetic DNA, 1 μg/ml) for the indicated times. IFN induction in the culture supernatant were assayed by IFN bioassay.

(G) Purified OASL-V5 were mixed and incubated with either control His-SUMO or His-SUMOcGAS proteins followed by Ni-NTA pull-down in presence or absence of (100 bp synthetic DNA, 1 μg/ml). Pulled-down proteins were detected by IB as indicated.

Representative results are shown from at least three times repeated experiments.

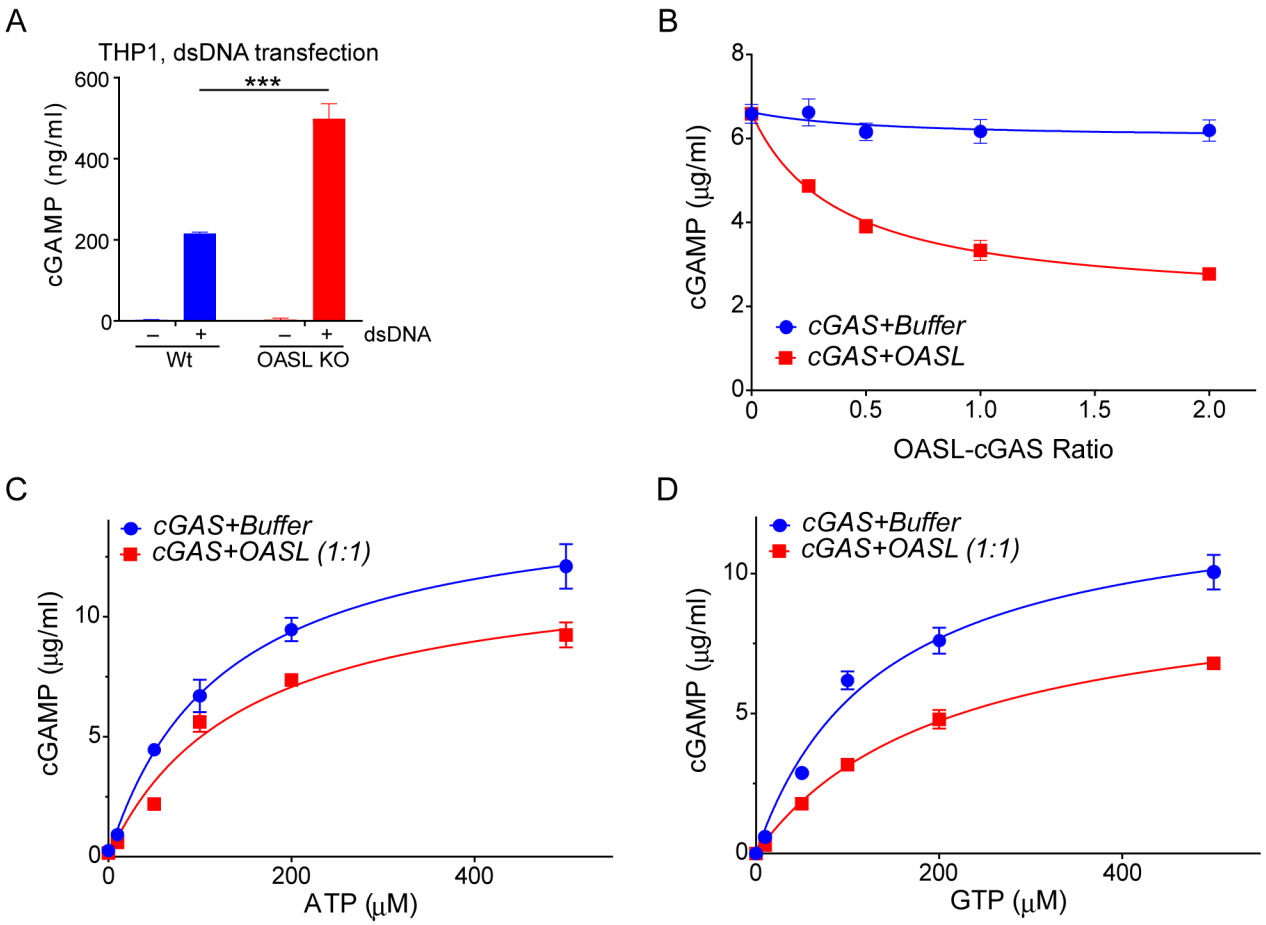

Fig. 6: Influence of OASL on cGAMP production.

(A) Indicated cells were stimulated with dsDNA (100 bp synthetic DNA, 1 µg/ml) for 16 h followed by cGAMP quantitation in cell lysates by mass spectroscopy.

(B) Purified OASL or buffer were mixed with purified cGAS proteins at indicated molar ratios and incubated on ice for 15 min followed by cGAS activity measurements by mass spectroscopy.

(C) and (D) Non-competitive inhibition of cGAS activity by OASL. Purified cGAS and OASL proteins were mixed at 1:1 molar ratio followed by cGAS activity assays either in presence of constant GTP (C) or ATP (D). For each experiment cumulative results from three biological repeats are shown.